7878 *Biochemistry* **2009,** *48,* 7878–7891
DOI: 10.1021/bi9006447

BIOCHEMISTRY
including biophysical chemistry & molecular biology
Article

The Partial Substrate Dethiaacetyl-Coenzyme A Mimics All Critical Carbon Acid Reactions in the Condensation Half-Reaction Catalyzed by *Thermoplasma acidophilum* Citrate Synthase[†]

Linda C. Kurz,[‡] Charles Z. Constantine,[§] Hong Jiang,[§] and T. Joseph Kappock*,[‖]

[‡]*Department of Biochemistry and Molecular Biophysics, Washington University School of Medicine, St. Louis, Missouri 63110,* [§]*Department of Chemistry, Washington University, St. Louis, Missouri 63130, and* [‖]*Department of Biochemistry, Purdue University, West Lafayette, Indiana 47907-2063*

Received April 15, 2009; Revised Manuscript Received June 27, 2009

ABSTRACT: Citrate synthase (CS) performs two half-reactions: the mechanistically intriguing condensation of acetyl-CoA with oxaloacetate (OAA) to form citryl-CoA and the subsequent, slower hydrolysis of citryl-CoA that generally dominates steady-state kinetics. The condensation reaction requires the abstraction of a proton from the methyl carbon of acetyl-CoA to generate a reactive enolate intermediate. The carbanion of that intermediate then attacks the OAA carbonyl to furnish citryl-CoA, the initial product. Using stopped-flow and steady-state fluorescence methods, kinetic substrate isotope effects, and mutagenesis of active site residues, we show that all of the processes that occur in the condensation half-reaction performed by *Thermoplasma acidophilum* citrate synthase (*Tp*CS) with the natural thioester substrate, acetyl-CoA, also occur with the ketone inhibitor dethiaacetyl-CoA. Free energy profiles demonstrate that the nonhydrolyzable product of the condensation reaction, dethiacitryl-CoA, forms a particularly stable complex with *Tp*CS but not pig heart CS.

Citrate synthase (CS)[1] catalyzes two half-reactions: a Claisen/aldol condensation reaction between acetyl-coenzyme A and oxaloacetate (OAA) that forms citryl-CoA and a hydrolysis reaction that releases citrate and CoA. In the condensation reaction, the terminal methyl group of acetyl-CoA is deprotonated to allow nucleophilic attack on the highly polarized OAA carbonyl (Figure 1). The subsequent hydrolysis reaction is thought to provide the thermodynamic driving force for citrate formation (*1*). Therefore, it is surprising (and often forgotten) that citryl-CoA hydrolysis is the slowest step in steady-state turnover, for both pig CS (PCS) (*2*) and *Thermoplasma acidophilum* CS (*Tp*CS), and that citryl-CoA hydrolysis nearly completely determines k_{cat} for *Tp*CS (*3*).

The mechanistically intriguing condensation reaction (Figure 1) involves both thermodynamic and kinetic challenges to proton abstraction, since carbon acids are weak and have large activation energy barriers. The pK_a values of the carbon acid (acetyl thioester) range above 21 (in H_2O) (*11*), while those of the abstracting base (carboxylic acid) are near 4, an apparent mismatch with $\Delta\Delta G \geq 23$ kcal/mol. A study of small molecule proton transfer rates in aqueous solution demonstrates that proton transfers from carbon are typically 10^9 slower than those from heteroatom acids of the same pK_a (*12*). CS must substantially stabilize the acetyl-CoA enolate, an intermediate with significant carbanion character, to overcome these obstacles (*13*). Asp317 (*Tp*CS numbering) removes a terminal methyl proton to form the enolate, and then several residues stabilize the terminal carbanion (*14*, *15*). A central goal of the current study is to understand how this proton transfer is performed.

Attempts to understand the functions of the important active site residues have been hampered by the fact that mutations inevitably affect both half-reactions, which have not been unravelled by varying conditions (*5*, *16*). For PCS, this task is made more difficult by the lack of convenient spectroscopic probes for enzyme intermediates. We show here that *Tp*CS and dethiaacetyl-CoA can be used to determine the roles of several conserved active site residues in the condensation half-reaction (Figure 1).

The partial CS substrate dethiaacetyl-CoA allows us to isolate the condensation half-reaction. The present work presents pre-steady-state studies of the condensation half-reaction, including the crucial proton transfer to Asp317 and the final condensation of the carbanion with OAA. Dethiaacetyl-CoA differs from acetyl-CoA by the replacement of the sulfur with a methylene group (Figure 2), which prevents hydrolysis. It is an apparent competitive inhibitor of PCS (K_i = 16 μM) (*17*). Dethiaacetyl-CoA undergoes CS-catalyzed terminal methyl H → D exchange (HDX) in D_2O (*7*), a reaction that is not observed during the turnover of acetyl-CoA in D_2O (for either PCS or *Tp*CS) (*3*). With PCS·OAA, dethiaacetyl-CoA is a better HDX substrate than propionyl-CoA and much better than acetonyl-CoA (Figure 2) (*7*). For all CS forms studied, the rate of dethiaacetyl-CoA HDX is close to k_{cat}. The similarity of the two rates

[†]This work was supported by grants from the National Institutes of Health to L.C.K. (GM 33851) and from the National Science Foundation to T.J.K. (MCB 0936108).

*Corresponding author. Phone: (765) 494-8383. Fax: (765) 494-1897. E-mail: kappock@purdue.edu.

[1]Abbreviations: *Aa*CS, citrate synthase from *Acetobacter aceti*; acetyl-CoA, acetyl-coenzyme A; AMX, amidocarboxymethyldethia-CoA; CAMCoA, carboxyamidomethyl-coenzyme A; CD, circular dichroism; CMCoA, carboxymethyl-coenzyme A; CMX, carboxymethyldethiacoenzyme A; dethiaacetyl-CoA, dethiaacetyl-coenzyme A; CS, citrate synthase; HDX, H → D exchange; OAA, oxaloacetate; IEF, isoelectric focusing; PCS, citrate synthase from pig heart; PDB, Protein Data Bank; SFF, stopped-flow fluorescence emission spectroscopy; *Tp*CS, citrate synthase from *Thermoplasma acidophilum*; TM, W245F-W115F-W17F triple mutant of *Tp*CS, containing a single Trp, W348.

 Published on Web 07/31/2009

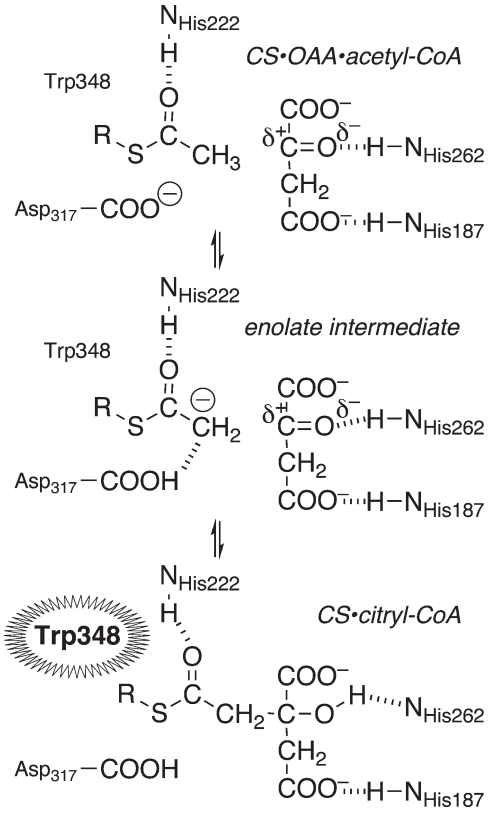

FIGURE 1: A working hypothesis for the CS condensation half-reaction. R is the remainder of CoA. The configuration and expected functions of *Tp*CS active site residues are similar to analogous PCS residues (given in parentheses) (*4*, *5*): Asp317 (Asp375) is the active site base that deprotonates acetyl-CoA during the CS condensation, His187 (His238) is a nearly pure OAA binding residue (*6*), His222 (His274) interacts directly with the thioester substrate and its enolate, and His262 (His320) plays an indirect role (*7*) (unpublished observations). The potential of His262 to function as a general acid during the alcohol-forming step is unclear. IEF analysis of His → Asn mutants (data not shown), crystal structures of CS complexes (*8*), and pK_a computations (*9*, *10*) (L. C. Kurz, unpublished results) all indicate that His262 equivalents are neutral in all characterized CS complexes. Trp348 is primarily responsible for the intrinsic fluorescence of *Tp*CS, which is strongly quenched in the presence of OAA (*6*). The complex with citryl-CoA has even higher fluorescence than the unliganded enzyme.

indicates that dethiaacetyl-CoA is a poorer substrate for the condensation half-reaction than acetyl-CoA, because k_{cat} is dominated by the citryl-CoA hydrolysis half-reaction for both *Tp*CS and PCS. HDX has been thought to imply dethiaacetyl-CoA enolate formation (*3*, *7*). While this appears to be the case for PCS, a different situation obtains for *Tp*CS. At a minimum, HDX requires reversible proton transfer, whatever the lifetime of a discrete enolate intermediate.

The main finding of this work is that a stable *Tp*CS·dethiacitryl-CoA complex is formed in solution. The nonhydrolyzable condensation product dethiacitryl-CoA has not been detected in reaction mixtures analyzed by ^{13}C NMR (PCS) (*7*, *3*) or ESI-MS (*Tp*CS) (S. A. Kerfoot, unpublished observations). However, dethiaacetyl-CoA has been shown to undergo the condensation reaction in the solid state: a crystal structure of *Tp*CS crystallized in the presence of saturating concentrations of OAA and dethiaacetyl-CoA contains only dethiacitryl-CoA at the active site [Protein Data Bank (PDB) entry 2r9e (C. Lehmann et al., unpublished observations)]. It seems likely that no more than 1 equiv of dethiacitryl-CoA is formed by *Tp*CS·OAA. In contrast,

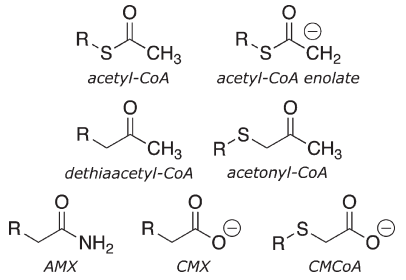

FIGURE 2: Acetyl-CoA, acetyl-CoA enolate, and analogues mentioned in this study. CMCoA and CMX are tight-binding analogues of the acetyl-CoA enolate (*17*−*19*). R is the remainder of CoA.

PCS forms a stable, unreacted PCS·OAA·dethiaacetyl-CoA complex in solution (*7*), a difference that can be understood by comparing free energy reaction profiles for the two CS forms presented here.

To an unusual degree, it is possible to link the fluorescence properties of Trp348 with the catalytic strategy of *Tp*CS (*6*). We exploit this in the present study of the condensation half-reaction performed by *Tp*CS. *Tp*CS contains four Trp residues: Trp17, Trp115, and Trp348 are located in the large domain and Trp245 is in the small domain. Mutagenesis has shown that Trp348 is the primary emitter (*6*). Trp348 is immobilized in a hydrophobic pocket 9 Å from OAA within binary (*Tp*CS·OAA) and ternary complexes (*Tp*CS·OAA plus an acetyl-CoA analogue). Despite being a dianion, OAA strongly quenches the intrinsic fluorescence emission of *Tp*CS due to excited-state electron transfer from Trp348 to the highly polarized OAA carbonyl. TM, a triply mutated *Tp*CS (W17F-W115F-W245F) containing only Trp348, has fluorescence properties that respond like the wild-type protein to ligand interactions but in a simplified manner. Thus, *Tp*CS or TM fluorescence increases when OAA is no longer present (i.e., upon its conversion to citryl-CoA).

Here we show that a fluorescence increase that is triggered by the addition of dethiaacetyl-CoA to *Tp*CS·OAA results from the destruction of OAA (the primary quencher of Trp348 fluorescence) and is consistent with the formation in solution of the *Tp*CS·dethiacitryl-CoA complex. All aspects of the condensation half-reaction can now be studied using *Tp*CS and dethiaacetyl-CoA.

EXPERIMENTAL PROCEDURES

Materials and Methods. All chemicals were obtained from Sigma-Aldrich or Fisher in the highest grade available and were used without further purification. Carboxamidomethyl-CoA (CAMCoA), carboxymethyl-coenzyme A (CMCoA), and citryl-CoA were prepared as described (*18*−*20*). [D_3]Acetyl-CoA, in which the terminal methyl group is fully deuterated, was prepared as described (*3*). Dethiaacetyl-CoA was prepared as described (*21*). The *Tp*CS-expressing pRec7-ArCS plasmid (*3*) was mutated with a QuikChange kit (Stratagene) and oligodeoxynucleotides (Supporting Information, Table S1) from IDT to furnish plasmids pJK381 (D317G-*Tp*CS) and pJK382 (D317N-*Tp*CS). For experiments in D_2O solutions, the pD was calculated from the pH meter reading (calibrated with standards in H_2O) by adding 0.4 (*22*).

Enzyme Isolation and Characterization. *Tp*CS and mutants were expressed, isolated, and assayed for enzyme activity (20 °C) as previously described (*3*, *6*). All enzyme concentrations are given assuming one active site per subunit.

Analytical Procedures. Electrospray ionization mass spectrometry (ESI-MS) was used to determine molecular masses of *Tp*CS forms to an accuracy of 3 Da. Protein concentrations were measured using 280 nm extinction coefficients established by stoichiometric active site titration of the *Tp*CS·OAA complex with the tight-binding inhibitor, CMCoA (*3*). OAA, citryl-CoA, and acetyl-CoA concentrations were measured using CS enzymatic end point assays. Isoelectric focusing was performed as previously described (*6*).

Absorbance, fluorescence, and circular dichroism (CD) spectra were recorded at 20 °C in 50 mM EPPS, pH 8, and 0.1 mM EDTA and analyzed as previously described (*3*). The equation used for CD titrations was as described previously (*19*). Steady-state fluorescence spectra for ligand titrations and quantum yield determinations were recorded on a Photon Technology International (PTI) Alphascan spectrofluorometer with excitation at 295 nm and emission scanning at ≥305 nm as described (*6*). Cell contents were stirred continuously to minimize adsorption artifacts. No photodegradation was observed. Fluorescence titrations were done by recording the emission intensity at the wavelength of maximum difference (usually 315 nm) between reactants and products, previously determined from steady-state spectra. Counts were collected for a time sufficient to reach an acceptable signal-to-noise ratio after each addition. Ligand (L) dissociation constants (K_d) were obtained from nonlinear least-squares fitting of the data to an equation that accounts for L depletion (eq 1).

$$F = F_0 + \frac{\Delta}{2}\{([L]+[E]_0+K_d) - \sqrt{([L]+[E]_0+K_d)^2 - 4[L][E]_0}\} \quad (1)$$

[D_3]Dethiaacetyl-CoA, in which the terminal methyl group is fully deuterated, was prepared by incubation of a concentrated stock solution of dethiaacetyl-CoA in D_2O buffer in the presence of a catalytic amount of *Tp*CS and OAA for at least 5 exchange half-lives. For stopped-flow fluorescence (SFF) experiments in D_2O, this stock solution was further diluted such that the amount of enzyme in the substrate/ligand syringe was less than 1% of that in the enzyme syringe.

Kinetic Analysis of Dethiaacetyl-CoA Complex Formation with D317G-TpCS·OAA. Complexation of dethiaacetyl-CoA by D317G-*Tp*CS·OAA was monitored by an initial velocity method. First, the rate of increase of the fluorescence emission intensity at 315 nm, in arbitrary units of counts per minute (cpm), was recorded using a PTI spectrofluorometer. A varying amount of dethiaacetyl-CoA was added to a solution containing final concentrations of 0.5 μM D317G-*Tp*CS and 75 μM OAA, 50 mM EPPS, pH 8, and 0.1 mM EDTA previously equilibrated at 20 °C, and the initial rate of the resulting fluorescence increase (in units of counts per minute per second) was recorded. Second, an extent spectrum and a fluorescence response factor for the D317G-*Tp*CS·OAA·dethiaacetyl-CoA complex product were obtained in a separate experiment, in which 0.5 mM dethiaacetyl-CoA was added to a preequilibrated mixture of 2 μM D317G-*Tp*CS and 75 μM OAA. The resulting fluorescence emission spectrum was recorded periodically until spectra taken 19 min apart showed a difference in intensity of less than ~0.1%. The intensity difference between the final extent spectrum and the initial (quenched) D317G-*Tp*CS·OAA complex spectrum was used to obtain a conversion factor relating counts per minute and micromolar product formed. Third, initial velocities of product complex formation were obtained (in units of micromolar product formed per second) from the 0.5 μM *Tp*CS data and then converted into specific initial velocities [v; units of (micromolar product per second)/(micromolar D317G-*Tp*CS)]. The maximum rate of the fluorescence increase, k_{max}, was obtained by fitting specific initial velocities to eq 2.

$$v = \frac{k_{max}[L]}{K_{app}+[L]} \quad (2)$$

H→D Exchange (HDX) Kinetics. D317G-*Tp*CS-mediated HDX of the terminal methyl protons of dethiaacetyl-CoA in D_2O was monitored by ^1H NMR with minor modifications of the procedure we used previously (*7*). NMR spectra were recorded at 25 °C at 500 MHz (^1H) on a Varian Inova 500 spectrometer equipped with a 5 mm Varian reverse probe. Longitudinal relaxation times (T_1) measured on the same instrument were used to select data acquisition paarameters. Spectra were collected with 90° pluses and a 12 s delay between acquisitions, $5T_1$ for the slowest-relaxing protons (2.38 s), on the terminal methyl group. Every 60 min, a spectrum averaging 32 transients was collected. Residual water signals were suppressed using continuous transmitter presaturation on the water signal during the delay between acquisitions.

Optical Analysis of Citryl-CoA-Dependent Turnover. Progress curves were recorded at 20 °C in EPPS/EDTA buffer at pH 8 using a PTI spectrofluorometer or a Cary3 spectrophotometer. Reactions initiated by the addition of excess citryl-CoA to *Tp*CS were monitored by either fluorescence emission intensity (excitation at 295 nm, emission monitored at 315 nm) or the thioester absorbance at 236 nm. A fluorescence titration of *Tp*CS·CoA with OAA was also performed.

Stopped-Flow Fluorescence (SFF) Kinetics. SFF progress curves were recorded at 20 °C using an Applied Photophysics SFMV12 stopped-flow apparatus, with a fluorescence cell excitation path length of 2 mm and emission path length of 10 mm. Intrinsic protein fluorescence excited at 285 nm was detected with a 305 nm high-pass filter (Schott glass WG305 filter) with 9.3 nm slit widths. All concentrations are given after mixing of an equal volume from each syringe.

Single-turnover experiments, with *Tp*CS·OAA present in excess over acetyl-CoA, used higher *Tp*CS concentrations to improve signal/noise and ensure single-turnover conditions and employed lower [OAA] to minimize inner-filter effects. A typical experiment contained 2 μM *Tp*CS, 40 μM OAA, and 0.1−0.4 μM acetyl-CoA in EPPS/EDTA buffer at pH 8. Pseudo-first-order conditions were achieved for the fast phase. Progress curves in single-turnover experiments were fit to a two-exponential expression to extract rate constants k_{obs1} (fast phase) and k_{obs2} (slow phase).

In dethiaacetyl-CoA complexation experiments, one syringe contained CS and OAA, the latter at saturating levels (≥20K_d), and the other contained dethiaacetyl-CoA at varying concentrations. All solutions were prepared in EPPS/EDTA buffer. Experiments designed to detect saturation of the rate of the first step of dethiaacetyl-CoA complexation (*vide infra*) used low *Tp*CS concentrations (0.03 μM) and lower dethiaacetyl-CoA concentrations. Progress curves were fit to a single-exponential expression to obtain rate constants (k_{obs}). Independently, Dynafit 3 (BioKin) (*23*) was used to fit progress curves directly, using a single differential fluorescence response factor and initial offsets as additional variables.

Table 1: Ligand Dissociation Constants (K_d) for *Tp*CS and Several Mutants[a]

form	OAA (μM)[b]	dethiaacetyl-CoA (μM)[c]
wild type	1.3[d]	1.47 ± 0.04
		1.64 ± 0.09[e]
TM	1.2[d]	8.9 ± 0.3
H187Q	~600[d]	< 0.1[f]
H222Q	33[d]	5.9 ± 1.3
H262Q	42[d]	0.68 ± 0.03
D317G	~0.012	NM[g]
D317N	0.38	NM[g]
W348Y	0.9[d]	1.86 ± 0.09

[a] Determined at 20 °C using a fluorescence titration of the indicated *Tp*CS form, except where noted. [b] Determined using the unliganded enzyme form. [c] Determined using the OAA complex of the indicated enzyme form. [d] From ref *6*. [e] Determined by CD titration of *Tp*CS·OAA. [f] This value is difficult to measure owing to a substantial inner filter effect from the high [OAA] required. [g] NM, not measurable, due to slow fluorescence change discussed in the text.

RESULTS

TpCS: Asp317 Mutants. We created mutants in the *Tp*CS active site base Asp317, which is known to remove the acetyl-CoA methyl proton (*5*, *8*, *24*−*28*), to learn if it has parallel roles in acetyl-CoA condensation half-reaction (Figure 1) and in reactions with dethiaacetyl-CoA. ESI-MS analysis showed the expected masses (minus Met1) for *Tp*CS (42943 observed; 42941.2 expected), D317G-*Tp*CS (42885 observed, 42883.1 expected), and D317N-*Tp*CS (42943 observed, 42940.2 expected). The absolute quantum yield for D317N-*Tp*CS is 0.14 (295 nm excitation), which is close to the wild-type *Tp*CS value, 0.15 (*3*). In contrast, the absolute quantum yield for D317G-*Tp*CS is lower (0.11). The quenched OAA complex spectrum is similar for all three forms, with quantum yields of 50%, 67%, and 44%, relative to unliganded *Tp*CS, D317G-*Tp*CS, and D317N-*Tp*CS, respectively. Fluorescence quenching due to OAA binding allowed the determination of dissociation constants (Table 1) that demonstrate an increased affinity of the D317X-*Tp*CS mutants for substrates, as was previously observed for the analogous PCS Asp375 mutants (*29*).

Isoelectric focusing (IEF) gels confirmed the purity of the D317X-*Tp*CS preparations, but they showed an unexpectedly low isoelectric point (p*I*) for each (Supporting Information, Figure S1). Substitution of a negatively charged Asp with a neutral residue would be expected to increase the p*I* of each mutant. However, isoelectric focusing reveals that native D317G-*Tp*CS and D317N-*Tp*CS have p*I* values (~8.8) between *Tp*CS (8.9) and TM (8.6). A comparable analysis performed using D12N-*Tp*CS, a mutant that lacks a surface-exposed negative residue, shows the expected shift to a higher p*I* value than *Tp*CS (9.1; data not shown).

Mutagenesis of the active site base Asp317 nearly or completely eliminates CS activity (Table 2, line 1). The relatively higher specific activity of D317G-*Tp*CS with citryl-CoA is notable because it indicates that the hydrolysis reaction is not rate-limiting, as it is for wild-type *Tp*CS (*3*). However, even this hydrolysis activity is substantially impaired (~2300-fold lower than wild-type *Tp*CS).

TpCS: Other Mutants. Three active site His residues have supporting roles in the condensation half-reaction (Figure 1). Alteration of any His decreases OAA affinity (Table 1), which is substantially lower for H187Q-*Tp*CS (*6*), but effects on dethiaacetyl-CoA affinity are modest.

Table 2: Summary of Rate Constants for Processes Involving Ternary Complex Formation[a]

process	substrate(s) or ligand(s)	*Tp*CS	D317G-*Tp*CS	D317N-*Tp*CS
k_{cat}[b]	OAA + acetyl-CoA	9.2[c]	0.0015	~0.0001[d]
hydrolysis[e]	*S*-citryl-CoA	9.2[c]	0.004	ND[f]
HDX[g]	OAA + dethiaacetyl-CoA	3.5	0.0004	ND
dequenching	OAA + dethiaacetyl-CoA	42.5[h]	0.0025[i]	ND

[a] In units of s^{-1}. [b] Determined at 100 μM acetyl-CoA and 400 μM OAA at 20 °C in 50 mM EPPS, pH 8, and 0.1 mM EDTA. These concentrations are saturating in both acetyl-CoA and OAA. The acetyl-CoA concentration is below the threshold for substrate inhibition, a minor effect due to the preferred-order kinetic mechanism of CS (*30*). [c] From ref *3*. We observed preparation-to-preparation variability in *Tp*CS rate constants. When a rate comparison was an important aspect of a given experiment, the k_{cat} for *Tp*CS from the same batch was measured at as near in time as possible (an example is given in the legend of Figure S7, Supporting Information). [d] This k_{cat} value is very uncertain and could include a substantial contribution from nonspecific acetyl-CoA hydrolysis or the reaction of DTNB with proteins. The rate is too slow to make product isolation and analysis practical. (DTNB is not required for assays that monitor thioester consumption or citrate production, but the high protein concentrations required for these very low rates rendered absorbance-based assays of thioester disappearance at 232 nm impractical.) However, the rate was linear in enzyme concentration and required the presence of OAA. [e] Determined from the rate of citryl-CoA-dependent catalysis at 20 °C in 50 mM EPPS, pH 8, and 0.1 mM EDTA. Citryl-CoA was present at a saturating level ($\geq 5K_m$). [f] ND, not determined. [g] Determined by NMR at 1 mM OAA in 25 °C in 50 mM potassium phosphate, pD 7.9, in D_2O (Supporting Information Figure S2). The k_{cat} determined under these conditions is 3.0 s^{-1}. CS k_{cat} values determined in phosphate buffers are lower than those determined in EPPS buffer (G. Drysdale, unpublished observations). The k_{cat} value is also lower in D_2O due to a solvent isotope effect (*3*). [h] From Table 3. [i] From Figure 9.

The alteration of the primary emitter Trp348 does not affect ligand affinities (Table 1). The alteration of any Trp residue does not affect OAA binding. However, TM demonstrates lower affinities for (acetyl-)CoA analogues, due to the W17F mutation required (unpublished observations).

Equilibrium Properties of Dethiaacetyl-CoA Complexation: Effect on the Quenched Fluorescence of TpCS·OAA. There is nearly complete restoration of (unliganded) intrinsic *Tp*CS fluorescence following the addition of dethiaacetyl-CoA to preformed *Tp*CS·OAA binary complexes (Figure 3A). We refer to this as "dequenching". In contrast, ternary complexes formed with *Tp*CS, OAA, and all other "unreactive" acetyl-CoA analogues (CAMCoA, CMCoA, CoA, and acetonyl-CoA) remain substantially quenched in steady-state fluorescence spectra (ref *6* and L. C. Kurz, unpublished observations). [The citryl-CoA complex has been shown to have enhanced fluorescence (*6*).] Dethiaacetyl-CoA is the only CS inhibitor known to dequench the *Tp*CS·OAA complex. As demonstrated below, formation of a ternary complex from *Tp*CS·OAA and dethiaacetyl-CoA requires at least two steps: a prior equilibrium binding step followed by a step associated with proton transfer(s) and dequenching. We refer to this multistep process as dethiaacetyl-CoA complexation to distinguish it from a simple binding interaction.

At equilibrium, the OAA complexes of all *Tp*CS mutants possessing the primary emitter (Trp348) behave in a similar manner and have substantially quenched fluorescence that is relieved upon turnover. Dequenching is observed upon the addition of dethiaacetyl-CoA to TM·OAA, which contains only the primary emitter Trp348 (Figure 3A). Comparable fluorescence changes were also observed in complexes of *Tp*CS mutants that lack one active site His (H187Q-*Tp*CS, H222Q-*Tp*CS, or

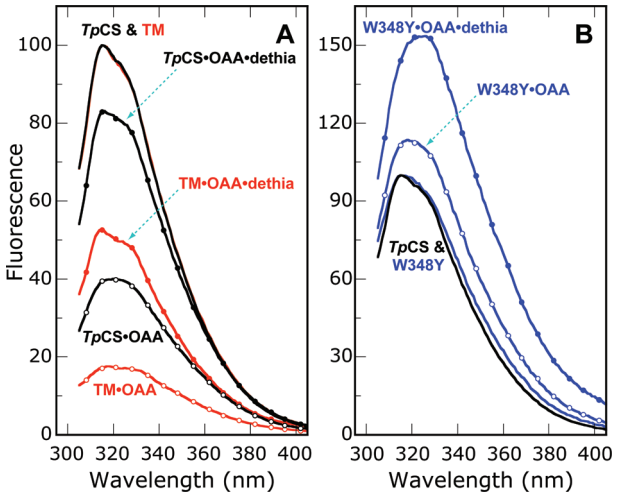

FIGURE 3: Fluorescence emission spectra of *Tp*CS, TM, and W348Y-*Tp*CS and their binary (E·OAA) or ternary (E·OAA·dethiaacetyl-CoA) complexes. (A) Comparison of wild-type *Tp*CS (black traces), which contains four Trp residues (17, 115, 245, and 348), and TM (red traces), a triple mutant, which contains only Trp348. The fluorescence of *Tp*CS forms containing Trp348 (*Tp*CS or TM) is quenched relative to unliganded enzyme (solid lines) by OAA binding (open circles). In contrast, the *Tp*CS·citryl-CoA complex shows *enhanced* fluorescence, relative to unliganded enzyme (*6*). At equilibrium, the ternary complex (filled circles) formed by *Tp*CS·OAA·dethiaacetyl-CoA is "dequenched"; that is, it shows reduced quenching. Note that *Tp*CS shows much less quenching in the binary and ternary complexes due to the presence of the secondary emitters Trp245, Trp115, and Trp17, which cause an increase in the fluorescence emission upon the addition of dethiaacetyl-CoA (panel B). The individual contributions of these three Trp residues to the fluorescence enhancement have not been dissected. (B) Spectrum of unliganded *Tp*CS (solid black line) compared to spectra of W348Y-*Tp*CS, a protein containing three Trp residues in which the primary emitter Trp348 has been replaced. Relative to unliganded W348Y-*Tp*CS (blue solid line), the binary (blue open circles) and ternary (blue filled circles) complexes show increased fluorescence emission intensity. The excitation wavelength was 295 nm. Emission spectra were recorded between 305 and 400 nm at 20 °C as described (*6*). Final concentrations were 1 μM subunit for each enzyme form, with 200 μM OAA, and 25 μM dethiaacetyl-CoA where indicated. Spectra recorded in the absence of ligands were normalized to have the same emission intensity (100 arbitrary units) at 315 nm. Every eighth data point is indicated by the symbols, but all data points are connected by lines that reflect the noise in the traces. The quantum yield of W348Y-*Tp*CS is substantially lower than that of *Tp*CS or TM, which is consistent with the role of Trp348 as the primary emitter (*6*).

H262Q-*Tp*CS; Supporting Information, Figure S3B−D). Although the final spectrum is reached only slowly, the addition of dethiaacetyl-CoA leads to dequenching of the D317G-*Tp*CS·OAA spectrum at equilibrium (Supporting Information, Figure S4). In contrast, a mutant lacking the primary emitter, W348Y-*Tp*CS, shows only a small fluorescence increase upon the binding of OAA (the opposite of what is observed with *Tp*CS forms that contain Trp348) and a further substantial fluorescence increase upon formation of the ternary complex containing dethiaacetyl-CoA (Figure 3B). All *Tp*CS Trp mutants except for W348Y-*Tp*CS show substantial quenching in CS·OAA binary complexes and are dequenched by the subsequent addition of dethiaacetyl-CoA.

Equilibrium Properties of Dethiaacetyl-CoA Complexation: Dissociation Constants. These fluorescence properties allow the determination of dethiaacetyl-CoA dissociation constants for *Tp*CS·OAA, which have also been measured using

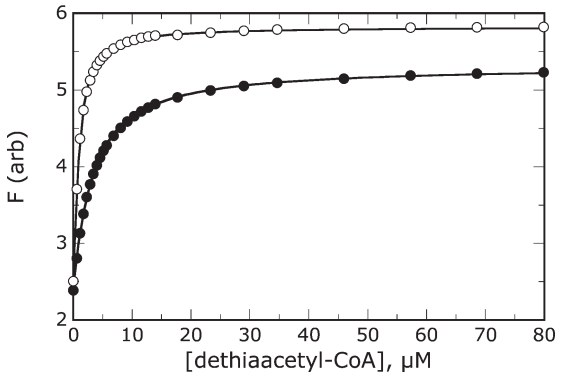

FIGURE 4: Fluorescence titrations of *Tp*CS·OAA with dethiaacetyl-CoA. Titrations of 1.0 μM *Tp*CS subunits in 200 μM OAA were performed at pL = 8.0 and 20 °C in H_2O (filled circles) or D_2O (open circles). The plotted values represent fluorescence emission intensity, in arbitrary units, at 315 nm. Solid lines are fits to eq 1 with K_d = 1.56 ± 0.04 μM (H_2O) or K_d = 0.35 ± 0.03 μM (D_2O), corresponding to an equilibrium solvent isotope effect of 4.5 ± 0.5.

lengthy CD titrations (*19*). Dethiaacetyl-CoA dissociation constants determined by fluorescence titrations of *Tp*CS·OAA forms that contain Asp317 (Figure 4 and Supporting Information, Figure S3) are given in Table 1. The value for *Tp*CS·OAA is comparable to a value of 1.6 μM obtained by CD titration (Supporting Information, Figure S5), which has been previously reported (*3*).

Comparable fluorescence changes were also observed in complexes of *Tp*CS mutants that lack an active site His (H187Q, H222Q, or H262Q), allowing determination of dethiaacetyl-CoA dissociation constants by fluorescence titration. At pH 8, the dethiaacetyl-CoA K_d is 6 μM for H222Q-*Tp*CS·OAA or 0.68 μM for H262Q-*Tp*CS·OAA (Supporting Information, Figure S3C,D). The dethiaacetyl-CoA affinity of H187Q-*Tp*CS appears to be even higher, but this is difficult to determine owing to the very low OAA affinity of this mutant (Supporting Information, Figure S3B). All three His mutants show impaired substrate binding, catalysis, or both, with k_{cat} values of 10 s^{-1} (H187Q-*Tp*CS), 0.006 s^{-1} (H222Q-*Tp*CS), or 0.7 s^{-1} (H262Q-*Tp*CS) at pH 8.

While the functions of His222 and Asp317 are linked (Figure 1), mutants in each residue are not equivalent. H222Q-*Tp*CS has a turnover rate slightly higher than D317G-*Tp*CS (Table 2), and it does not bind OAA or dethiaacetyl-CoA as tightly as D317G-*Tp*CS (Table 1). As there was an apparent time-dependent fluorescence change upon the addition of dethiaacetyl-CoA, determinations of its affinity for H222Q-*Tp*CS·OAA required slower addition of successive aliquots, with a 10 min equilibration period. This was faster than the equilibration time required for D317G-*Tp*CS (*vide infra*).

Equilibrium Properties of Dethiaacetyl-CoA Complexation: pH Effects and Comparison to CAMCoA. Acetonyl-CoA and CAMCoA, analogues that, like dethiaacetyl-CoA, have neutral termini, bind to PCS·OAA (*19*) or *Tp*CS·OAA (Figure 5) with little dependence on pL (pH or pD). Binding of CAMCoA to TM·OAA is somewhat tighter in D_2O, with an equilibrium solvent isotope effect of ~2 ($^{D_2O}K_d = K_d^{H_2O}/K_d^{D_2O}$) in the pL range of 7−9. The K_d for CAMCoA binding to TpCS·OAA measured by CD titration is 1.78 ± 0.03 μM at pH 8 with a similar $^{D_2O}K_d$. (There is little or no fluorescence change associated with CAMCoA or acetonyl-CoA binding, so only CD titrations were used.)

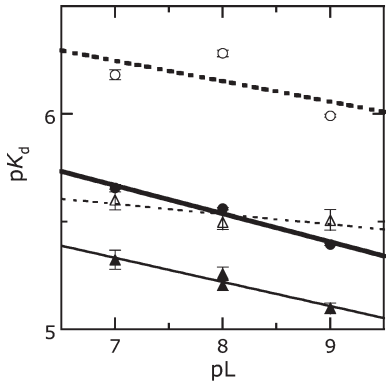

FIGURE 5: pL dependence of K_d values for two neutral-terminus acetyl-CoA analogues. *Tp*CS was used to measure the dethiaacetyl-CoA affinity, while TM was used to measure the CAMCoA affinity. While TM binds CoA analogues more loosely than *Tp*CS, there are otherwise no meaningful differences between these two enzyme forms (*6*). The K_d values for dethiaacetyl-CoA complex formation with *Tp*CS·OAA (filled circles, in H_2O; open circles, in D_2O) were determined by fluorescence titrations. The K_d values for CAMCoA binding to TM·OAA (filled triangles, in H_2O; open triangles, in D_2O) were determined by CD titrations. For both analogues, pK_d values show little dependence on pL. Dethiaacetyl-CoA unweighted linear fits give slope -0.13 ± 0.02 in H_2O (thick solid line; $R^2 = 0.976$) and -0.10 ± 0.11 in D_2O (thick dashed line; $R^2 = 0.418$). The ratio of fitted values gives a solvent isotope effect (SIE) range for dethiaacetyl-CoA complexation of 3.8−4.5, from pL 7 to pL 9. CAMCoA unweighted linear fits give slope -0.11 ± 0.02 in H_2O (thin solid line; $R^2 = 0.930$) and -0.05 ± 0.03 in D_2O (thin dotted line; $R^2 = 0.685$). The ratio of fitted values gives a SIE range for CAMCoA binding of 1.8−2.4, from pL 7 to pL 9. Error bars indicate the fitting uncertainty in each pK_d determination. A replicate determination for CAMCoA at pH 8 is shown. Note that the ordinate scale is half that of the abscissa.

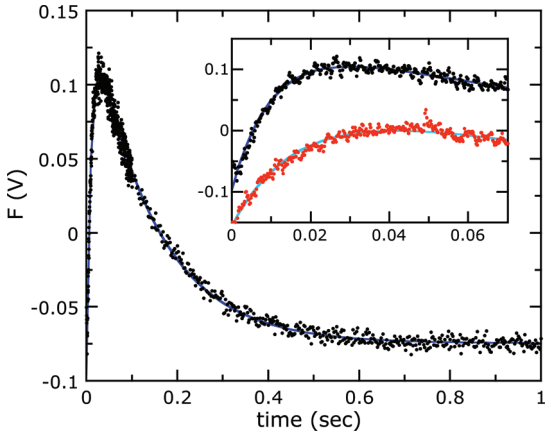

FIGURE 6: Reaction of *Tp*CS·OAA with substoichiometric acetyl-CoA monitored by stopped-flow fluorescence spectroscopy (SFF). *Tp*CS preincubated with OAA in one syringe was mixed with acetyl-CoA in the other, giving initial concentrations of 2 μM *Tp*CS, 40 μM OAA, and 0.2 μM acetyl-CoA. The solid blue line is a fit of the data to a two-exponential equation with $k_{obs1} = 96.4 \pm 1.4$ s^{-1} and $k_{obs2} = 7.23 \pm 0.08$ s^{-1}. In a parallel experiment under steady-state conditions, the *Tp*CS k_{cat} was determined to be 6.8 s^{-1} at saturating acetyl-CoA and OAA. *Inset*, An enlargement of the fast phase of the reaction comparing acetyl-CoA (black symbols) with [D_3]acetyl-CoA (red symbols). The light blue solid line shows a fit of the [D_3]acetyl-CoA data to a two-exponential equation with $k_{obs1} = 58.5 \pm 0.9$ s^{-1} and $k_{obs2} = 7.2 \pm 0.1$ s^{-1}. Concentration dependence data for these observed rates are presented in Supporting Information, Figure S7. The [D_3]acetyl-CoA data have been shifted vertically by −0.1 V.

Titrations of *Tp*CS·OAA with dethiaacetyl-CoA are unavoidably associated with rapid HDX, so that the titrant is presumed to be [D_3]dethiaacetyl-CoA in D_2O. The affinity of dethiaacetyl-CoA was substantially higher in D_2O than in H_2O, yielding an unusually large inverse equilibrium solvent isotope effect of ~4 (Figure 4).

Net proton uptake is apparently not required for dethiaacetyl-CoA complexation. Neither the dethiaacetyl-CoA affinity nor the equilibrium solvent isotope effect has a profound dependence on pL (Figure 5). This contrasts with the binding of acetyl-CoA analogues that have anionic carboxylate termini (CMCoA or CMX) to PCS·OAA, *Tp*CS·OAA, or TM·OAA, which is accompanied by proton uptake; plots like Figure 5 with these analogues have slopes near one (ref *19* and unpublished observations).

Other Processes Relieving OAA Quenching: Formation of TpCS·Citryl-CoA. Citryl-CoA binding has been shown to increase *Tp*CS fluorescence, to ~120% of the unliganded *Tp*CS emission intensity; the *Tp*CS·citryl-CoA complex quantum yield is higher than that for unliganded *Tp*CS (*6*). Citryl-CoA hydrolysis by *Tp*CS is rate-limiting in the steady state (*3*). In steady-state, multiple-turnover experiments, we expect the *Tp*CS·citryl-CoA complex to be the predominant form of the enzyme. During citryl-CoA-dependent turnover, fluorescence should rapidly rise and remain roughly constant until the substrates are exhausted. In a single-turnover experiment with acetyl-CoA as the substrate, we would expect initial formation of citryl-CoA and a transient increase of *Tp*CS fluorescence (a detailed explanation is given in Supporting Information). These expectations are met.

First, the addition of excess citryl-CoA to *Tp*CS results in a large fluorescence increase of the expected magnitude, followed by a sharp decrease as citryl-CoA is used up and OAA-mediated quenching is established (Supporting Information, Figure S6). While not initially present in the reaction, a small amount of OAA is formed, together with acetyl-CoA, by the reverse-condensation reaction. These substrates accumulate until the tighter binding citryl-CoA is consumed, at which point they too are converted to products. At the end of the experiment, only *Tp*CS, citrate, and CoA remain so the initial *Tp*CS fluorescence is restored.

Second, the reaction of acetyl-CoA with excess *Tp*CS·OAA shows a rapid, transient fluorescence increase followed by a slower decrease to the baseline, OAA-quenched fluorescence (Figure 6). Each phase is a single-exponential process, with rate constants k_{obs1} (acetyl-CoA → citryl-CoA) or k_{obs2} (citryl-CoA destruction). The fluorescence decrease in the second phase is due to rapid rebinding of OAA after product dissociation (as detailed in Supporting Information), and k_{obs2} is identical to the steady-state k_{cat} determined under these conditions with the same enzyme sample (*6*). An experiment with [D_3]acetyl-CoA (Figure 6, inset) shows a normal substrate isotope effect (1.7 ± 0.2) for k_{obs1} but not k_{obs2} (1.00 ± 0.09). We note that no explicit solution is available for a multistep process of this complexity, which involves a binding step, two kinetically significant chemical steps, and complications arising from dead-end complex formation with CoA and/or OAA.

In summary, all equilibrium and kinetic experiments are consistent with the proposition that binding of acetyl-CoA and its conversion to citryl-CoA relieves OAA-mediated quenching simply because the acceptor for electron transfer from the excited indole, the OAA carbonyl, is no longer present.

Dynamic Properties of Dethiaacetyl-CoA Complexation: TpCS·OAA-Mediated HDX. Wild-type *Tp*CS·OAA catalyzes HDX at the same rate as acetyl-CoA-dependent turnover (*3*), which is slower in the presence of phosphate and D_2O

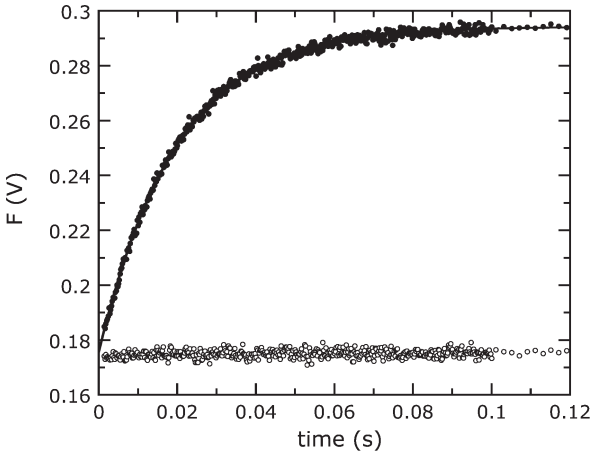

FIGURE 7: Reaction of *Tp*CS·OAA with excess dethiaacetyl-CoA monitored by SFF. After mixing, the reaction contained 0.2 μM *Tp*CS, 100 μM OAA, and 40 μM dethiaacetyl-CoA (filled circles) at 20 °C and pH 8.0. The solid line is a single-exponential fit to the data with $k_{obs} = 50.8 \pm 0.1$ s^{-1}. A control reaction lacking only dethiaacetyl-CoA shows no fluorescence changes (open circles). A depiction of the complete progress curve showing fitting residuals with a logarithmic time basis is given in Supporting Information, Figure S8.

(Table 2). As expected for a mutant enzyme lacking a key active site base, D317G-*Tp*CS-mediated HDX and acetyl-CoA-dependent turnover rates are ~10^{-5} that of wild-type *Tp*CS (Table 2). For comparison, the analogous D375G-PCS·OAA HDX rate is similarly reduced, to $< 1.3 \times 10^{-5}$ that of wild-type PCS (*7*).

Dynamic Properties of Dethiaacetyl-CoA Complexation: Stopped-Flow Fluorescence (SFF) Analysis. Static spectra show that the addition of dethiaacetyl-CoA to the quenched *Tp*CS·OAA complex restores most of the fluorescence intensity of *Tp*CS alone (Figure 3). SFF analysis shows a monophasic fluorescence increase associated with dethiaacetyl-CoA complex formation with *Tp*CS·OAA (Figure 7). The data are fit well by a single-exponential expression, with an observed rate (k_{obs}) that saturates at high concentrations. These observations require a model involving a minimum of two steps (Scheme 1), the first of which apparently occurs in the dead time of the instrument and is associated with a negligible fluorescence change. Therefore, the interaction of dethiaacetyl-CoA (L) with preformed CS·OAA complexes (E) was treated as a two-step process, with an initial rapid equilibrium binding process followed by a first-order isomerization of the EL complex, described by dissociation constants K_{d1} ($=k_{-1}/k_1$) and K_{d2} ($=k_{-2}/k_2$). Values of k_{obs} determined at varied [dethiaacetyl-CoA] were fit to eq 3 (*31*).

$$k_{obs} = \frac{k_2[L]}{K_{d1} + [L]} + k_{-2} \quad (3)$$

Fluorescence increases upon ternary complex formation are first order in [dethiaacetyl-CoA] with *Tp*CS·OAA (Supporting Information, Figure S9). There is no missing amplitude in progress curves that might indicate additional silent steps required in the approach to equilibrium, indicating that a two-step kinetic model (Scheme 1) is sufficient to account for the complete binding interaction for *Tp*CS. Fits of rate data to eq 3 yielded $K_{d1} = 7.9 \pm 0.6$ μM, $k_2 = 40.9 \pm 0.6$ s^{-1}, and $k_{-2} = 16.3 \pm 0.8$ s^{-1}, for an overall $K_{d1}K_{d2} = 3.2$ μM (H_2O experiments). However, accompanying amplitude data were not reliably fit to a partner equation (a version of eq 10 in ref *31*). As suggested (*31*), we then searched for a lag in the progress curves by conducting experiments at lower *Tp*CS·OAA concentration but failed to obtain convincing evidence of a lag phase.

Scheme 1: Kinetic Model for Dethiaacetyl-CoA (L) Complex Formation with *Tp*CS·OAA (E)

$$E + L \underset{}{\overset{K_{d1}}{\rightleftharpoons}} EL \underset{k_{-2}}{\overset{k_2}{\rightleftharpoons}} EL^*$$

Table 3: Parameters from Global Fitting of SFF Studies of Dethiaacetyl-CoA Complex Formation with *Tp*CS·OAA

parameter	H_2O	D_2O	isotope effect[a]
K_{d1} (μM)	5.7	3.3	1.7[b]
k_2 (s^{-1})	43	28	1.5
k_{-2} (s^{-1})	13	6.4	2.0
$K_{d1}K_{d2}$ (μM)	1.7	0.74	2.3[b]

[a] Computed using the parameter for H_2O divided by that for D_2O (e.g., $K_{d1}^{H_2O}/K_{d1}^{D_2O}$). Experiments performed in D_2O used preexchanged [D_3]-dethiaacetyl-CoA, so the values presented combine solvent and substrate isotope effects. k_2 and k_{-2} are as discussed in the text. [b] The affinity of dethiaacetyl-CoA for *Tp*CS·OAA is greater in D_2O than in H_2O, so these are inverse isotope effects.

Global fitting of SFF progress curves allowed the incorporation of information from transient amplitudes. A good fit to the data was obtained using a single fluorescence response factor; i.e., only the formation of the dequenched complex (EL*) causes a change in fluorescence (Scheme 1). This can be rationalized by two considerations. First, there is negligible transient or equilibrium fluorescence change upon the binding of the carboxamide-terminated ("neutral") acetyl-CoA analogue CAMCoA to *Tp*CS (data not shown). Second, theoretical considerations (discussed below) indicate that only introduction of a discrete negative charge into the active site or the conversion of the OAA carbonyl to an alcohol can relieve OAA quenching of intrinsic *Tp*CS fluorescence (*6*). Analysis using eq 3 indicated a model of rapid preequilibrium binding, which cannot be directly simulated using DynaFit software. The initial rate of dethiaacetyl-CoA (L) binding, k_1, was therefore fixed at 1000 μM^{-1} s^{-1} and k_{-1} was allowed to vary. The fitted value for k_{-1} was used to obtain K_{d1}. Parameters obtained from global progress curve fits (Table 3) were in good agreement with those obtained from rate constant data alone using eq 3, for both H_2O and D_2O experiments (Figure 8 and Supporting Information, Figure S10). The combined dissociation constant derived from pre-steady-state kinetic analysis ($K_d = K_{d1}K_{d2}$) agreed well with dissociation constants determined by CD or fluorescence titrations in H_2O (Table 1). However, the derived equilibrium isotope effect ($^{D_2O}K_d$ of 2.3) was smaller than the large $^{D_2O}K_d$ value determined by titration (Figure 4). The reason for the discrepancy in the magnitude of these inverse isotope effects is not clear.

Dynamic Properties of Dethiaacetyl-CoA Complexation: Dethiaacetyl-CoA Slowly Dequenches D317G-TpCS·OAA. Preliminary experiments indicated it would be difficult to determine the affinity of dethiaacetyl-CoA for D317G-*Tp*CS·OAA because fluorescence changes were unacceptably slow at enzyme concentrations appropriate for titrations. While complex formation is a required prerequisite, fluorescence dequenching does not simply report on ternary complex formation and is likely to be affected by subsequent reaction(s).

We used a fluorescence kinetics method to estimate the affinity of dethiaacetyl-CoA for D317G-*Tp*CS·OAA and to compare the rate of dequenching with that of wild-type *Tp*CS. At high

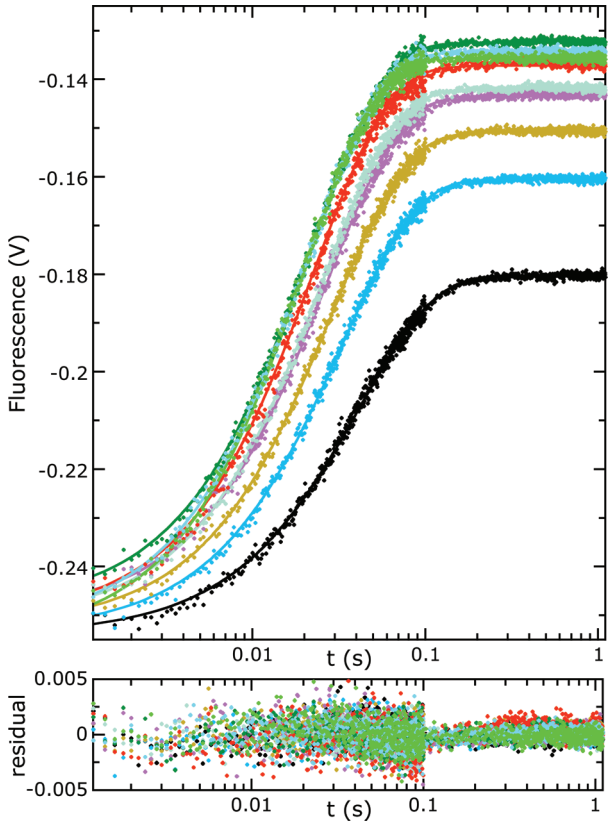

FIGURE 8: Semilogarithmic curves showing results of progress-curve fitting for *Tp*CS·OAA (0.2 μM final subunit concentration) complex formation with dethiaacetyl-CoA in H_2O. After mixing, the reaction contained 0.2 μM *Tp*CS, 100 μM OAA, and variable dethiaacetyl-CoA at 20 °C and pH 8.0. Data points are shown as small symbols, and fits are shown as solid lines of the same color. From bottom to top (at 1 s), the traces were obtained at 2.05 (black), 4.12, 6.17, 8.23, 10.28, 15.42, 40.14, 30.86, or 20.57 (dark green) μM dethiaacetyl-CoA; note that the last three are out of order due to small differences in the initial offsets. Fit residuals are at the bottom.

concentrations of *Tp*CS·OAA (2 μM) and dethiaacetyl-CoA (500 μM), saturation was attained within ~30 min, which allowed determination of a ternary complex spectrum and estimation of a fluorescence response factor (Supporting Information, Figure S4). These ligand-dependent fluorescence changes are like other *Tp*CS forms that contain Trp348: OAA quenches fluorescence, while the subsequent addition of dethiaacetyl-CoA restores it, albeit quite slowly for D317G-*Tp*CS.

The initial velocity of the fluorescence increase associated with ternary complex formation was used to construct a kinetic saturation curve (Figure 9). The maximal rate of complexation (k_{max}) is comparable to the rate of acetyl-CoA- and citryl-CoA-dependent turnover by D317G-*Tp*CS and somewhat faster than HDX (phosphate and D_2O inhibition exaggerates the true difference in rates).[2] The low rate of acetyl-CoA-dependent

[2]The K_{app} derived from these experiments suggests that a looser dethiaacetyl-CoA complex is formed with D317G-*Tp*CS·OAA, relative to wild-type *Tp*CS·OAA. However, it is a composite value that represents contributions from both binding and kinetic processes, and it is not possible to define it in terms of the equilibrium and rate constants. Furthermore, the possibility of a change in mechanism exists for D317X-*Tp*CS mutants. Unlike *Tp*CS, it appears possible that enolate formation and condensation are less tightly coupled because the catalytic base and active site geometry are inevitably altered in these mutants.

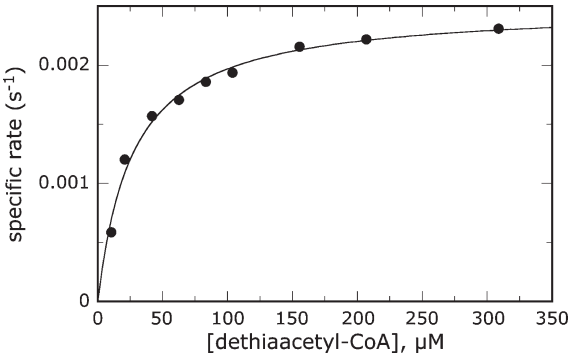

FIGURE 9: Initial rate of the fluorescence increase associated with dethiaacetyl-CoA complex formation with D317G-*Tp*CS·OAA. Dethiaacetyl-CoA was added to 0.5 μM D317G-*Tp*CS subunits previously equilibrated in 75 μM OAA at pH 8.0 and 20 °C. The appearance of the full fluorescence change (monitored at 315 nm) at each [dethiaacetyl-CoA] is very slow, so it was impractical to wait until the reaction had reached completion. The specific initial rate for the formation of the fluorescence-enhanced product resulting from dethiaacetyl-CoA complex formation with *Tp*CS·OAA was computed as described in Experimental Procedures. The solid line is a fit of eq 2 to the data that yields $k_{max} = (2.50 \pm 0.06) \times 10^{-3}$ s^{-1} and $K_{app} = 27 \pm 3$ μM.

turnover in D317G-*Tp*CS is consistent with the widely accepted conclusion that Asp317 accepts the proton removed from the acetyl-CoA methyl group during the condensation reaction (*3*, *19*, *24*, *26*, *29*). The parallel suppression of the dethiaacetyl-CoA HDX rate in D317G-*Tp*CS demonstrates that Asp317, assisted by other parts of the catalytic apparatus, has a similar function during dethiaacetyl-CoA complexation.

There is a possibility that dethiaacetyl-CoA complexation of D317G-*Tp*CS might be irreversible. Like D375G-PCS (*7*), D317G-*Tp*CS binds ligands very tightly (Table 1 and unpublished observations). The reversibility of ternary D317G-*Tp*CS·OAA·dethiaacetyl-CoA complex formation was assessed using CMCoA as a kinetic trap. The binding of CMCoA is very tight (the K_d for its dissociation from *Tp*CS·OAA is about 23 nM), and it forms a ternary complex that is less fluorescent than the dethiaacetyl-CoA ternary complex (*6*). A slow diminution of fluorescence intensity was observed upon the addition of CMCoA to the preformed dethiaacetyl-CoA ternary complex, with a trapping $t_{1/2}$ of several hours (data not shown). This observation indicates that dissociation of dethiaacetyl-CoA from D317G-*Tp*CS·OAA can occur but it is very slow.

DISCUSSION

Our working hypothesis is that the interaction of dethiaacetyl-CoA with *Tp*CS·OAA is that of a complete substrate for the CS condensation half-reaction. Here we place the new findings in the rich context of what is already known about the mechanism of CS and outline future work that is now possible.

Oxaloacetate (OAA) Binding Site and the Origin of OAA Quenching. The electron-deficient OAA carbonyl carbon effectively quenches tryptophan fluorescence by electron transfer from the excited indole of Trp348 (*20*). This phenomenon depends upon the presence of OAA within the active site and is closely linked to the active site environment necessary for efficient catalysis. OAA is highly polarized when bound to CS (*32*, *33*). The large positive electrostatic potential within or near the active site pocket is generated by several Arg residues and is a factor for

both the enolate intermediate and the polarized OAA carbonyl (*6*, *34*). It promotes excited-state electron transfer from Trp348 in the quenching interaction to the dianonic OAA acceptor that would otherwise be very unfavorable. This feature makes possible the kinetic studies reported here.

OAA polarization may also increase its reactivity for nucleophilic attack by the acetyl-CoA enolate. An alternative suggestion based on computations is that OAA carbonyl polarization stabilizes the enolate intermediate without increasing carbonyl reactivity (*34*). In either view, OAA carbonyl polarization promotes the CS condensation reaction while providing an unusually incisive spectroscopic probe into its mechanism.

Citryl-CoA Formation Causes Dequenching. The fluorescence emission from the *Tp*CS·citryl-CoA complex is enhanced relative to unliganded *Tp*CS and is substantially enhanced relative to the quenched *Tp*CS·OAA complex (Supporting Information, Figure S6, and ref *6*). Kinetic considerations indicate that the *Tp*CS·citryl-CoA complex accumulates during steady-state turnover with citryl-CoA as the substrate (*6*). In single-turnover experiments with acetyl-CoA and OAA as substrates, we have identified conditions in which *Tp*CS·citryl-CoA is the predominant enzyme form (Figure 6). The enhanced fluorescence of this complex decays with a rate constant equal to k_{cat} in steady-state experiment controls. The majority of the dequenching observed upon the *Tp*CS·OAA→*Tp*CS·citryl-CoA conversion is explained by the chemical conversion of the OAA carbonyl, which destroys its ability to quench Trp348 fluorescence.

Origin of Dequenching Triggered by the Interaction of Dethiaacetyl-CoA with TpCS·OAA. Formation of the complex between dethiaacetyl-CoA and *Tp*CS·OAA is uniquely correlated with a fluorescence increase that can be used to monitor complexation equilibria and kinetics (Figures 4 and 7). Other inhibitory CoA analogues do not dequench the *Tp*CS·OAA complex, even those that are believed to be analogues of the enolate intermediate (Figure 2).

A wealth of structural and spectroscopic data is available for CS binary or ternary complexes with small molecules that resemble substrates, transition states, or intermediates. CS ternary complex crystal structures solved with OAA and one of several acetyl-CoA analogues, including CMCoA, CMX, or amidocarboxymethyldethia-CoA (AMX) (*21*, *26*, *28*, *35*, *36*) (C. Lehmann et al., unpublished observations; PDB entry 2r26), show that the acetyl-CoA methyl terminus binds near the active site base (*Tp*CS Asp317) (*25*). These structures were the first indication that the side chain of this residue (rather than the nearby His222) is the active base. The binding of CMCoA, CMX, AMX, or CAMCoA to CS·OAA has little or no effect on the *Tp*CS·OAA fluorescence spectrum, indicating that they do not interfere with OAA-mediated quenching. Complexes that unambiguously do not contain OAA, such as the *Tp*CS·CoA, *Tp*CS·citrate, or *Tp*CS·citrate·CoA complexes, have fluorescence intensities similar to that of the unliganded enzyme. All complexes known to contain unreacted OAA are quenched.

The simplest hypothesis consistent with the data is that the fluorescence enhancement observed upon dethiaacetyl-CoA complex formation with *Tp*CS·OAA is the result of the destruction of OAA. The same phenomenon is observed in both wild-type *Tp*CS and TM, indicating that OAA, a powerful quencher of Trp348 fluorescence, is no longer present in the active site. Just as in the condensation of OAA with acetyl-CoA to form citryl-CoA results in fluorescence enhancement, dethiaacetyl-CoA reacts to form dethiacitryl-CoA.

We discount the possibility that dequenching is caused by insertion into the active site of a negative charge, such as the acetyl-CoA enolate (Figure 1, middle panel). A reorientation of negative charges within the active site could diminish the ability of OAA to function as an electron acceptor by depolarizing the OAA carbonyl (*6*); calculations of this unusual electron transfer from the excited indole to a dianion acceptor demonstrate a high degree of sensitivity to electrostatic fields within the active site (ref *6* and P. Callis, personal communication). The acetyl-CoA enolate is structurally analogous to CMCoA or CMX (Figure 2), which form isoelectronic ternary complexes because tight binding of anionic-terminus analogues requires uptake of a single proton from solution (*19*, *27*). Crystallographic and solid-state NMR studies show that CMX forms a short hydrogen bond with Asp317 (*21*, *27*, *28*) and that the shared proton in the short hydrogen bond resides mainly on the side chain of this active site base (*27*). A similar configuration is expected in the enolate intermediate: the proton resides mainly on the active site base while the charge resides mainly on the acetyl-CoA enolate (*15*). Difference spectra show that the binding of CMCoA causes only a small steady-state fluorescence change with *Tp*CS·OAA and none at all with TM·OAA (*6*). Therefore, enolate formation is not likely to account for the observed dequenching neither during the conversion of acetyl-CoA to citryl-CoA nor in the dequenching triggered by dethiaacetyl-CoA complexation.

The Active Site Base Asp317 Participates in Dethiaacetyl-CoA Complexation. Mutations that affect the rate of catalysis by affecting the generation and stabilization of the reactive enolate also affect the rate of fluorescence increase observed on dethiaacetyl-CoA reaction with *Tp*CS·OAA. PCS Asp375 has a key role in catalysis and HDX, which are linked, as demonstrated by a parallel suppression in rates with various D375X-PCS mutants (*7*). In addition to affecting the rates of catalysis and HDX, the corresponding mutations in *Tp*CS (D317G-*Tp*CS, D317N-*Tp*CS) also affect the rate of dequenching (Table 2), a phenomenon that does not occur in PCS.[3]

These observations indicate that the active site base Asp317 has an important role in the rapid formation of a complex that displays the final dequenched fluorescence, rapid turnover, and HDX. A simple substrate analogue complex (ground-state analogue) is unlikely to explain all of these observations. SFF studies of dethiaacetyl-CoA complex formation with *Tp*CS·OAA reveal an apparent rapid prior equilibrium associated with little or no change in fluorescence, followed by rate-limiting dequenching (Figure 8). A 220000-fold slower fluorescence increase was observed with D317G-*Tp*CS·OAA (Figure 9 and Table 3) paralleling the effect of this mutation on catalysis and HDX.

Ligands adhere tightly to D317G-*Tp*CS (Table 1). However, dethiaacetyl-CoA can dissociate from the complex formed with D317G-*Tp*CS·OAA, as demonstrated by multiple-turnover HDX (Supporting Information, Figure S2) and a CMCoA trapping experiment. Additional evidence for slow ligand release

[3]The catalytic activity of D317G-*Tp*CS is significantly higher than that of D317N-*Tp*CS. Only D317G-*Tp*CS is unambiguously functional in all three linked processes: substrate turnover, HDX, and dequenching. Rates with D317N-*Tp*CS are so low as to be very difficult to study. The smaller Gly side chain in D317G-*Tp*CS might allow it to use a somewhat different mechanism than does wild-type *Tp*CS, a consideration that highlights the complexity of the CS system and the need for cautious interpretation of mutant data.

is that dequenching caused by dethiaacetyl-CoA complexation is somewhat faster than the steady-state rates of HDX or acetyl-CoA-dependent catalysis (Table 3), each of which requires ligand dissociation.

Asp317 and His222 appear to work together to generate and stabilize the acetyl-CoA enolate, although H222Q-*Tp*CS may be slightly less impaired than D317G-*Tp*CS. An important future task is to assess the roles of these residues in each half-reaction.

Parallel Substrate Kinetic Isotope Effects on Catalysis and Dethiaacetyl-CoA Complexation. The intrinsic isotope effect for proton transfer from acetyl-CoA with PCS is near 2 (*37*). This intrinsic isotope effect is derived from a difficult intramolecular competition experiment utilizing H,D,T-labeled acetyl-CoA, and there is considerable uncertainty in its value. However, the value of the primary isotope effect is clearly much smaller than the ~6 expected for symmetric proton transfers and is consistent with the late transition state expected for the production of an unstable enolate intermediate (uphill free energy change) (*38*, *39*).

A semiquantitative analysis of the two phases observed in single-turnover SFF studies with acetyl-CoA (Figure 6) is possible. The second phase is a fluorescence decrease with a rate constant (k_{obs2}) identical to k_{cat} and that demonstrates no substrate isotope effect, as expected for the hydrolysis of the high-fluorescence *Tp*CS·citryl-CoA complex. The first phase (k_{obs1}), which is associated with increasing fluorescence and represents the formation of citryl-CoA, appears to include contributions from proton transfer, the condensation half-reaction, and acetyl-CoA binding. However, the observed substrate isotope effect ($^{D}k_{obs1}$) is very close in value to that measured by intramolecular competition (*37*). This clearly indicates a substantial contribution from isotopically sensitive proton transfer to k_{obs1}. The magnitude of the effect also suggests that proton transfer is close to rate-determining for the condensation half-reaction or is concerted with it.[4] In contrast, the linear dependence of k_{obs1} on [*Tp*CS·OAA] (Supporting Information, Figure S7C) suggests that the acetyl-CoA binding process predominates at higher *Tp*CS·OAA concentrations.

By analogy, if the fluorescence increase that accompanies the dethiaacetyl-CoA reaction with *Tp*CS·OAA represents the entire condensation half-reaction, we would expect to see primary isotope effects of about the same magnitude for the condensation reaction with acetyl-CoA and for the dequenching associated with dethiaacetyl-CoA complexation. That expectation is met (Table 3).

However, the interpretation of these data is slightly more complex than the straightforward interpretation of acetyl-CoA substrate isotope effects. For both *Tp*CS·OAA and PCS·OAA, no exchange of the methyl protons of acetyl-CoA with solvent deuterons is observed during turnover (*3*). However, the methyl protons of dethiaacetyl-CoA readily undergo CS-catalyzed exchange in D_2O. To avoid complications due to partial exchange, SFF experiments performed in D_2O used preexchanged [D_3]-dethiaacetyl-CoA. This substitution does not introduce difficulty into the interpretation of steps involving covalent bond changes in the condensation half-reaction, for which no solvent isotope effect is expected. However, as discussed below, we could not avoid a substantial solvent equilibrium isotope effect.

[4]In the condensation reaction, proton transfer to form the enolate may be concerted with carbon−carbon bond formation, or it may occur in a separate, prior step. In the related enzyme malate synthase, enolate formation occurs in a separate step that precedes carbon−carbon bond formation; i.e., the enolate intermediate has a discrete lifetime (*40*).

For acetyl-CoA, there is a strict segregation of substrate and solvent isotope effects on the two half-reactions that comprise k_{cat}. A comparison of steady-state substrate and solvent isotope effects indicates that the former affect only the condensation reaction while the latter affect only the hydrolysis reaction (*3*). The steady-state substrate isotope effect for deuterium substitution in the methyl group of acetyl-CoA ($^{D}V_{acetyl\text{-}CoA}$) is 1.17 in either H_2O or D_2O (*3*), showing that the substrate and solvent isotope effects occur in separate steps. Because the slow hydrolysis step dominates in k_{cat}, the steady-state substrate isotope effect, $^{D}V_{acetyl\text{-}CoA}$, is smaller than $^{D}k_{obs1}$ observed in single-turnover experiments with acetyl-CoA and smaller than the intrinsic isotope effect derived from intramolecular competiton experiments (*37*). Although the SFF studies of the reaction of dethiaacetyl-CoA are free of complications from the solvent isotope effects on hydrolysis, they inevitably incorporate both solvent effects on complexation and the expected substrate isotope effects for covalent bond changes in the condensation half-reaction.

Substantial inverse solvent isotope effects (Figure 5) are observed for the formation of CoA analogue complexes with *Tp*CS·OAA, so the observed values for dethiaacetyl-CoA report on both solvent and substrate isotope effects (Table 3). The isotope effect on the first step ($^{D_2O}K_{d1}$), a rapid equilibrium associated with initial binding, can be attributed to protein conformational changes and ligand-dependent displacement of protein-bound waters. The isotope effect on the second step ($^{D_2O}K_{d2}$), which is associated with dequenching, is inverse (1.31 ± 0.02; that is, tighter binding in D_2O) and of smaller magnitude than the opposing normal kinetic isotope effects on k_2 and k_{-2}. It probably represents an equilibrium substrate isotope effect on chemical steps.

Proton transfers are therefore involved in the second step as we see a primary substrate isotope effect of the expected magnitude. However, these proton transfers are internal (the proton transfer event does not involve proton uptake or release from bulk solution) as indicated by the shallow pL dependence of the K_d values for neutral-terminus acetyl-CoA analogues (Figure 5).

Comparison of CS Forms. CS has a highly conserved active site and a basic dimeric architecture that is found in both dimeric (PCS and *Tp*CS) and hexameric forms [for instance, *Acetobacter aceti* CS (*Aa*CS), which is a trimer of dimers (*21*)]. However, there is variability in the kinetic parameters and substrate dissociation constants, as might be expected for an ancient enzyme, with roles in both energy metabolism and biosynthesis, that is harbored by organisms adapted to a wide variety of environmental pressures. For example, the K_d for OAA is 0.86 μM for *Tp*CS (*3*) and 17 μM for *Aa*CS (*21*). These differences may be partly due to protein conformational changes that occur at each step in the CS reaction, which could differ substantially in dimers and hexamers. *Aa*CS has a Trp residue in a position equivalent to *Tp*CS Trp348 that shows fluorescence responses comparable to those described here, with some intriguing differences in the initial complexation of dethiaacetyl-CoA (H. Jiang, unpublished observations). This confirms that the fluorescence phenomena described here are not simply a peculiar feature of *Tp*CS.

PCS will not be the primary vehicle for future mechanistic study of the CS condensation half-reaction. This system does not allow a deconvolution of the effects a mutation (or change in reaction conditions) has on the condensation and hydrolysis half-reactions (*16*). PCS also does not have OAA-dependent fluorescence changes, probably because it lacks a Trp residue in the

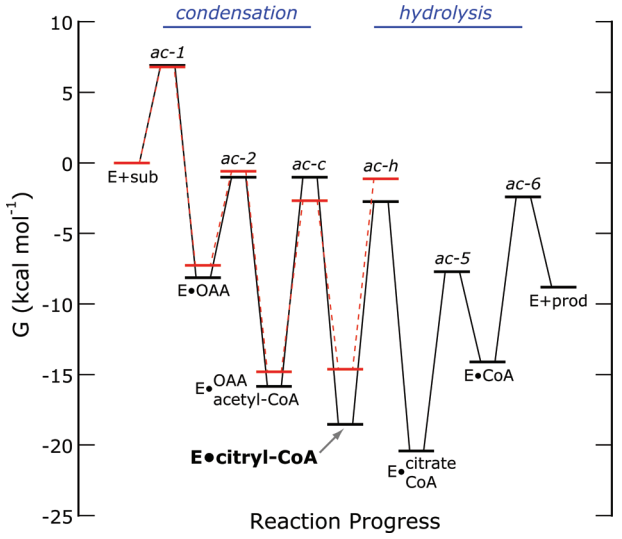

FIGURE 10: Free energy reaction profiles. The full *Tp*CS profile (pH 8 and 20 °C) is in black, and the partial PCS profile (pH 8.2 and 26.5 °C) is in red. The free energy of the enzyme and the free substrates has been arbitrarily assigned a value of zero. Other energy levels, including the activated complexes for each reaction (ac), are given relative to this using a 1 M standard state for reactants with pure water given an activity of 1. Free substrates or products are not listed for the intermediate states, but do contribute to the free energy of each. The free energy values (Supporting Information, Table S2 and Table S3) and the method of their determination are detailed in Supporting Information.

equivalent position to *Tp*CS Trp348, needed for transient kinetic studies like those reported here. Finally, as we demonstrate in the next section, PCS does not preferentially stabilize the condensation product.

TpCS Selectively Stabilizes Citryl-CoA. The available kinetic and thermodynamic information allow the estimation of ΔG and $\Delta G^{\ddagger}$ values for all six binding equilibria and catalytic steps in the *Tp*CS reaction (Supporting Information, Table S2) and the assembly, for the first time, of a nearly complete free energy reaction profile at pH 8 and 20 °C (Figure 10). The profile combines previously published (*3*) and new data, and its construction required several assumptions described in detail in the Supporting Information. The overall ΔG for the CS reaction at pH 8.00 and 20 °C is the sum of ΔG values for six individual reactions, −8.8 kcal/mol. These assumptions introduce a fair amount of uncertainty into the values of ΔG and $\Delta G^{\ddagger}$. Despite this, the computed value is close to the overall ΔG of −9.0 kcal/mol measured for the citrate synthase reaction at pH 7.0 and 38 °C (*1*). Even though some uncertainties do remain in the *Tp*CS energy diagram, the key points relevant to the current discussion, in particular, the striking stabilization of the *Tp*CS·citryl-CoA complex, will not be affected by future refinements.

A reaction energy diagram for PCS was based on data obtained under slightly different conditions (*2*). The data available for the PCS profile end at the citryl-CoA hydrolysis step. In PCS, the ternary substrate complex (PCS·OAA·acetyl-CoA) is the most stable prehydrolysis state.

In contrast, the *Tp*CS profile clearly shows that the most stable prehydrolysis state is the *Tp*CS·citryl-CoA complex, with the unambiguously rate-limiting hydrolysis reaction favored over reverse condensation (Figure 10). This complex is in a much deeper energetic well than PCS·citryl-CoA. Catalysis by *Tp*CS is also unambiguously rate-limited by hydrolysis and is slower than PCS, even at its 70 °C "normal" operating temperature. It is worth noting that the excess stabilization of the citryl-CoA intermediate in the *Tp*CS system is less at higher temperatures (*3*). The deep well for citryl-CoA explains the kinetic stabilization of citryl-CoA by *Tp*CS evident in steady-state (Supporting Information, Figure S6) and single-turnover (Figure 6) kinetic analyses. If hydrolysis were somehow blocked (as it is for dethiaacetyl-CoA), the *Tp*CS·dethiacitryl-CoA condensation product would accumulate.

We have presented evidence that dethiacitryl-CoA is the product of the interaction of *Tp*CS·OAA with dethiaacetyl-CoA. The failure to detect dethiacitryl-CoA formation from [2-^{13}C]OAA by ^{13}C NMR in PCS solutions was puzzling and might be due to intermediate-NMR chemical shift exchange regime effects (*7*). However, we now believe any dethiacitryl-CoA that is formed by PCS would be below the level of detection by this relatively insensitive method. If the free energy levels for the reaction of dethiaacetyl-CoA parallel those with the natural substrate acetyl-CoA, the PCS·dethiacitryl-CoA complex (Figure 10) should be present at a much lower concentration than the PCS·OAA dethiaacetyl-CoA ground-state complex. For *Tp*CS, the condensation product should be the predominant complex species.

At first this seems surprising, as all CS forms are thought to use a common chemical mechanism. However, the rates of catalysis and the on-enzyme equilibria (the relative stabilities of enzyme-bound species) depend on the CS form being examined (*3*). This makes it possible to study the condensation and hydrolysis half-reactions independently, by pairing the appropriate CS and CoA analogue.

Dethiacitryl-CoA Production Alters the Interpretation of HDX Experiments. In typical assay conditions, dethiaacetyl-CoA behaves as if it is a moderately potent, competitive, reversible CS inhibitor (*17*), not an alternate substrate. Dethiacitryl-CoA formation has not been previously detected in solution (ref *7* and S. A. Kerfoot, unpublished observations). However, dethiaacetyl-CoA has been unambiguously shown to be a substrate for the condensation half-reaction by the recent crystallographic detection of a stoichiometric *Tp*CS·dethiacitryl-CoA complex (C. Lehmann et al., unpublished observations; PDB entry 2r9e), and we have now presented evidence that this occurs in solution as well. This apparent paradox is resolved by our working hypothesis: dethiacitryl-CoA is reversibly generated in the *Tp*CS active site, forming up to 1 equiv of a tightly bound ligand that is not released intact into bulk solution.

Dethiaacetyl-CoA is the best known substrate for CS·OAA-mediated HDX, which interrogates proton transfers relevant to the condensation reaction (*7*). At a minimum, HDX requires enolate formation and exchange of the abstracted proton with bulk solvent. Alternatively, the kinetically preferred HDX mechanism could involve formation of a dethiacitryl-CoA intermediate, which then fragments with concomitant uptake of a deuteron to give [D_{n+1}]dethiaacetyl-CoA. Since the HDX reaction goes to completion, the second possibility would require both rapid reverse condensation and facile [D_n]dethiaacetyl-CoA dissociation, to allow fresh ligand to bind. Neither static fluorescence spectra nor SFF experiments can rule out the possibility that a small amount of a complex containing dethiaacetyl-CoA enolate accounts for all of the HDX activity. However, dissociation and rate constants derived from fluorescence studies (Tables 1 and 3) suggest that dethiacitryl-CoA is a kinetically competent intermediate in the HDX reaction.

First, *Tp*CS is mainly present as the dethiacitryl-CoA complex in the saturating conditions used for the HDX experiments, just as

it is in the near equilibrium represented by the *Tp*CS·dethiacitryl-CoA crystal structure. Based upon the measured kinetic and equilibrium constants (Table 3), 95% of bound dethiaacetyl-CoA is in the form of the final, dequenched complex (dethiacitryl-CoA). Second, global analysis yields rate constants for dethiaacetyl-CoA condensation and reverse condensation (k_2 and k_{-2}, respectively; Table 3) that are consistent with rapid, reversible dethiacitryl-CoA formation within the active site and with magnitudes that are consistent with the rate of HDX. Third, the steady progression of the HDX reaction is also evidence against irreversible dethiacitryl-CoA formation. A progressive decrease in HDX rate should occur if stoichiometric dethiacitryl-CoA were retained irreversibly at the active site, that is, if it functioned as a kind of suicide substrate. Fourth, dethiacitryl-CoA is a nonhydrolyzable, bisubstrate analogue that might be expected to be a potent CS inhibitor. (It has never, to our knowledge, been chemically synthesized or successfully extracted from CS to test this hypothesis.) If dethiacitryl-CoA were to form catalytically as a side product of the HDX reaction, i.e., in excess of the number of available active sites, one might again expect progressive inhibition of the HDX rate. However, there is no evidence for release of dethiacitryl-CoA into solution or any rate decrease during the HDX reaction performed by PCS or *Tp*CS (*3*, *7*). We propose that no more than 1 equiv of dethiacitryl-CoA is reversibly formed in the active site and it is never released into solution.

A Large Solvent Isotope Effect on Dethiaacetyl-CoA Complex Formation. The solvent isotope effect on dethiaacetyl-CoA affinity for *Tp*CS·OAA is inverse (tighter in D_2O) and is about 4, an unusually large value (Figures 4 and 5).[5]

Solvent isotope effects on the affinity of other neutral-terminus CoA analogues such as CAMCoA are smaller and close to 2 in the same pL range (Figure 5). Generally, equilibrium solvent isotope effects are attributable to differences in fractionation factors at exchangeable sites in reactants and products (*42*). The substitution of water−protein interactions with ligand−protein interactions and the displacement of water from the active site crevice by the acetyl-CoA analogue are likely contributors to a solvent isotope effect. These should be roughly similar for CAMCoA and dethiaacetyl-CoA. However, the former is a ground-state analogue (substrate) complex while the latter continues to react, forming an intermediate analogue complex. Given the necessarily greater affinity of an enzyme for an activated intermediate (analogue) than a ground-state analogue, it is reasonable to suppose some additional compaction and conformation changes may be associated with the tighter binding of intermediate (analogue) complexes. Since citryl-CoA binds very tightly to *Tp*CS, dethiacitryl-CoA should too. This would lead to the prediction that other intermediate analogue complexes, such as those with the enolate analogue CMCoA, might show unusually large inverse equilibrium isotope effects.[6]

Dethiaacetyl-CoA as a Probe of the Condensation Reaction. The dequenching phenomenon is a useful probe of the previously obscure condensation half-reaction, which is kinetically silent in steady-state experiments because it is ≥5 times faster than hydrolysis (*3*). The degree to which the interaction of acetyl-CoA with *Tp*CS·OAA resembles that with dethiaacetyl-CoA depends upon the relative degree of steric compatibility with the active site (Figure 2) and enolate reactivity, which is higher for thioester enolates (summarized in ref *7*).

A natural inference from the free energy diagram analysis (Figure 10) is that the most stable complex formed by dethiaacetyl-CoA with *Tp*CS·OAA would be *Tp*CS·dethiacitryl-CoA, a complex that cannot undergo hydrolysis. While this may be correct, it is inadvisible to draw too strong an analogy between the rates of citryl-CoA formation and fragmentation (k_c and k_{-c}, respectively, as detailed in Supporting Information) with the corresponding processes in dethiacitryl-CoA because of likely differences in enolate stability, ligand sterics, and the reaction conditions under which rate constants were determined. However, the rate of dequenching during acetyl-CoA-dependent turnover (k_{obs1}) is comparable to that for dequenching due to dethiaacetyl-CoA complexation (k_2). (Some difference is expected, presuming that the natural substrate acetyl-CoA has advantages in sterics and reactivity.) There is much less ambiguity in the interpretation of the dethiaacetyl-CoA titration experiments and thus in k_2. We propose that dethiaacetyl-CoA is the best available tool to study steps in the condensation half-reaction, one that will allow reliable comparisons of the reaction in wild-type *Tp*CS with that in mutants or under different experimental conditions.

Only one structure of a CS active site mutant is available (*5*), which is remarkable considering the many structures available for various CS forms, unliganded or in complexes, and the importance of CS conformational changes. The availability of a spectroscopic probe should motivate future combined structural and kinetic studies of *Tp*CS mutants.

Kinetic Importance of Asp317. Stabilization of the acetyl-CoA enolate by protein hydrogen bonds is thought to be the most important factor in reducing the barrier to proton transfer (*13*). Calculations specifically implicate hydrogen bonding in stabilization of the acetyl-CoA enolate on citrate synthase (*15*, *43*).

The linked condensation, HDX, and dequenching phenomena have a common dependence upon the *Tp*CS active site base Asp317, demonstrating its central role is to ensure rapid enolate formation. A short hydrogen bond, like that observed between Asp317 and carboxylate-terminus inhibitors (CMX and CMCoA), has the potential to explain how CS achieves a rapid proton abstraction from the terminal methyl of (dethia)acetyl-CoA during its binding and activation. In this view, opposing favorable (e.g., formation of a hydrogen bond) and unfavorable (e.g., steric clash) enthalpic effects leave the overall affinity unchanged but accelerate a sluggish proton transfer from carbon. Additional enhancement can be attributed to the positive electrostatic environment in the CS active site exerted by nearby Arg residues. These findings are congruent with concepts, advanced by Gerlt, Gassman, Cleland, and Kreevoy (*13*), that hydrogen bonding deployed within an active site can explain the ability of enzymes to achieve kinetically competent enolate formation.

[5]See the discussion in ref *41*. The solvent isotope effect on the K_d ($= K_{d1}K_{d2}$) derived from SFF analysis is inverse but not as large (Table 3). The apparent affinities from SFF and from titration analysis in H_2O are in excellent agreement, so the discrepancy appears to be associated with experiments performed in D_2O with [D_3]dethiaacetyl-CoA. Furthermore, until new data are obtained, we consider affinity values derived from direct titration experiments to be more reliable than those computed from six SFF parameters.

[6]This prediction has been verified (unpublished results). Anionic-terminus analogues CMCoA and CMX form a short hydrogen bond to Asp317, and it is possible that the structurally analogous dethiaacetyl-CoA enolate would too. However, this does not account for the isotope effect on dethiaacetyl-CoA complex formation, because short hydrogen bonds are associated with normal isotope effects (tighter in H_2O). The large inverse equilibrium isotope effects observed with both types of inhibitors are therefore doubly surprising.

CONCLUSIONS

The major challenge in the Claisen-like CS condensation reaction is the enolization of acetyl-CoA, which requires enzyme-catalyzed proton removal from a carbon acid. CS·OAA catalyzes H → D exchange (HDX) in the terminal methyl group of dethiaacetyl-CoA, a process requiring enolization and critical proton transfers relevant to the condensation reaction. The intrinsic fluorescence of *Tp*CS is strongly quenched by OAA but is mostly restored by the further addition of acetyl-CoA or dethiaacetyl-CoA, respectively leading to the formation of a transient complex with citryl-CoA or a stable complex with dethiacitryl-CoA, a nonhydrolyzable analogue.

Each complex shows fluorescence dequenching caused by the destruction of OAA, which is converted to enzyme-bound (dethia)citryl-CoA. A free energy reaction diagram indicates that *Tp*CS·citryl-CoA is the most stable prehydrolysis intermediate form of *Tp*CS. Therefore, the predominant product of the complexation of *Tp*CS·OAA by the nonhydrolyzable dethiaacetyl-CoA is expected to be the nonhydrolyzable *Tp*CS·dethiacitryl-CoA. Fluorescence changes are used to monitor complex formation at equilibrium and the condensation reaction in presteady-state experiments. Isotope and pH effects are consistent with internal proton transfer from the terminal methyl group of (dethia)acetyl-CoA to the active site base *Tp*CS Asp317. The magnitude of the observed substrate isotope effects is consistent with the idea that the proton transfer is rate-determining for condensation and that the enolate does not exist as a long-lived intermediate; proton abstraction and condensation may even be concerted. (Only difficult double-isotope effect experiments could completely resolve this question.) During steady-state turnover with acetyl-CoA as the substrate, these internal proton transfers and their attendant isotope effects are masked because the isotope-sensitive step does not contribute much to the observed rate. Thus, the reactions of dethiaacetyl-CoA with *Tp*CS·OAA can be used to study all steps of the CS condensation half-reaction.

ACKNOWLEDGMENT

We thank G. Drysdale for discussions, C. Frieden for comments on the manuscript, and D. G. Drueckhammer for advice on the synthesis of dethiaacetyl-CoA.

SUPPORTING INFORMATION AVAILABLE

Sequences of oligodeoxynucleotides used (Table S1); IEF of D317X-*Tp*CS mutants (Figure S1); NMR H → D exchange data for D317G-*Tp*CS (Figure S2); *Tp*CS mutant fluorescence titration data (Figure S3); fluorescence spectra for D317G-*Tp*CS·OAA following addition of dethiaacetyl-CoA and calculation of the fluorescence response factor for the product of that interaction (Figure S4); *Tp*CS·OAA + dethiaacetyl-CoA CD titration data (Figure S5); a multiple-turnover progress curve for the interaction of citryl-CoA with *Tp*CS (Figure S6); fluorescence amplitude and rate data for single-turnover experiments with acetyl-CoA and *Tp*CS·OAA (Figure S7); a semilogarithmic depiction of a progress curve for dethiaacetyl-CoA complex formation with *Tp*CS·OAA (Figure S8); a comparison of global and individual fits for dethiaacetyl-CoA complex formation with *Tp*CSetOAA (Figure S9); semilogarithmic depictions of global progress curves and fits for dethiaacetyl-CoA complex formation with *Tp*CS·OAA in D_2O (Figure S10); an appendix presenting the method used to construct free energy reaction profiles for *Tp*CS and PCS (Schemes S1 and S2, Tables S2 and S3). This material is available free of charge via the Internet at http://pubs.acs.org.

REFERENCES

1. Guynn, R. W., Gelberg, H. J., and Veech, R. L. (1973) Equilibrium constants of the malate dehydrogenase, citrate synthase, citrate lyase, and acetyl coenzyme A hydrolysis reactions under physiological conditions. *J. Biol. Chem. 248*, 6957–6965.
2. Pettersson, G., Lill, U., and Eggerer, H. (1989) Mechanism of interaction of citrate synthase with citryl-CoA. *Eur. J. Biochem. 182*, 119–124.
3. Kurz, L. C., Drysdale, G., Riley, M., Tomar, M. A., Chen, J., Russell, R. J. M., and Danson, M. J. (2000) Kinetics and mechanism of the citrate synthase from the thermophilic archaeon *Thermoplasma acidophilum*. *Biochemistry 39*, 2283–2296.
4. Russell, R. J. M., Hough, D. W., Danson, M. J., and Taylor, G. L. (1994) The crystal structure of citrate synthase from the thermophilic archaeon. *Thermoplasma acidophilum. Structure 2*, 1157–1167.
5. Evans, C. T., Kurz, L. C., Remington, S. J., and Srere, P. A. (1996) Active site mutants of pig citrate synthase: effects of mutations on the enzyme catalytic and structural properties. *Biochemistry 35*, 10661–10672.
6. Kurz, L. C., Fite, B., Jean, J., Park, J., Erpelding, T., and Callis, P. (2005) Photophysics of tryptophan fluorescence: link with the catalytic strategy of the citrate synthase from *Thermoplasma acidophilum*. *Biochemistry 44*, 1394–1413.
7. Kurz, L. C., Roble, J. H., Nakra, T., Drysdale, G. R., Buzan, J. M., Schwartz, B., and Drueckhammer, D. G. (1997) Ability of single-site mutants of citrate synthase to catalyze proton transfer from the methyl group of dethiaacetyl-coenzyme A, a non-thioester substrate analog. *Biochemistry 36*, 3981–3990.
8. Remington, S. J. (1992) Mechanisms of citrate synthase and related enzymes (triose phosphate isomerase and mandelate racemase). *Curr. Opin. Struct. Biol. 2*, 730–735.
9. Bas, D. C., Rogers, D. M., and Jensen, J. H. (2008) Very fast prediction and rationalization of pK_a values for protein-ligand complexes. *Proteins 73*, 765–83.
10. Li, H., Robertson, A. D., and Jensen, J. H. (2005) Very fast empirical prediction and rationalization of protein pK_a values. *Proteins 61*, 704–21.
11. Amyes, T. L., and Richard, J. P. (1992) Generation and stability of a simple thiol ester enolate in aqueous solution. *J. Am. Chem. Soc. 114*, 10297–10302.
12. Gerlt, J. A., and Gassman, P. G. (1993) Understanding the rates of certain enzyme-catalyzed reactions: proton abstraction from carbon acids, acyl-transfer reactions, and displacement reactions of phosphodiesters. *Biochemistry 32*, 11943–11952.
13. Gerlt, J. A. (2007) Enzyme catalysis of proton transfer at carbon atoms, in Hydrogen-transfer reactions (Hynes, J. T., Klinman, J. P., Limbach, H. H., and Schowen, R. L., Eds.) pp 1107−1138, Wiley-VCH, Weinheim, Germany.
14. Mulholland, A. J., and Richards, W. G. (1998) A model of the condensation step in the citrate synthase reaction. *J. Mol. Struct. (THEOCHEM) 427*, 175–184.
15. Donini, O., Darden, T., and Kollman, P. A. (2000) QM-FE calculations of aliphatic hydrogen abstraction in citrate synthase and in solution: reproduction of the effect of enzyme catalysis and demonstration that an enolate rather than an enol is formed. *J. Am. Chem. Soc. 122*, 12270–12280.
16. Kurz, L. C., Nakra, T., Stein, R., Plungkhen, W., Riley, M., Hsu, F., and Drysdale, G. R. (1998) Effects of changes in three catalytic residues on the relative stabilities of some of the intermediates and transition states in the citrate synthase reaction. *Biochemistry 37*, 9724–9737.
17. Martin, D. P., Bibart, R. T., and Drueckhammer, D. G. (1994) Synthesis of novel analogs of acetyl coenzyme A: mimics of enzyme reaction intermediates. *J. Am. Chem. Soc. 116*, 4660–4668.
18. Bayer, E., Bauer, B., and Eggerer, H. (1981) Evidence from inhibitor studies for conformational changes of citrate synthase. *Eur. J. Biochem. 120*, 155–160.
19. Kurz, L. C., Shah, S., Crane, B. R., Donald, L. J., Duckworth, H. W., and Drysdale, G. R. (1992) Proton uptake accompanies formation of the ternary complex of citrate synthase, oxaloacetate, and the transition-state analog inhibitor, carboxymethyl-CoA. Evidence that a neutral enol is the activated form of acetyl-CoA in the citrate synthase reaction. *Biochemistry 31*, 7899–7907.

20. Kurz, L. C., Shah, S., Frieden, C., Nakra, T., Stein, R. E., Drysdale, G. R., Evans, C. T., and Srere, P. A. (1995) Catalytic strategy of citrate synthase: subunit interactions revealed as a consequence of a single amino acid change in the oxaloacetate binding site. *Biochemistry 34*, 13278–13288.
21. Francois, J. A., Starks, C. M., Sivanuntakorn, S., Jiang, H., Ransome, A. E., Nam, J.-W., Constantine, C. Z., and Kappock, T. J. (2006) Structure of a NADH-insensitive hexameric citrate synthase that resists acid inactivation. *Biochemistry 45*, 13487–13499.
22. Glasoe, P. K., and Long, F. A. (1960) Use of glass electrodes to measure acidities in deuterium oxide. *J. Phys. Chem. 64*, 188–189.
23. Kuzmic, P. (1996) Program DYNAFIT for the analysis of enzyme kinetic data: application to HIV proteinase. *Anal. Biochem. 237*, 260–273.
24. Alter, G. M., Casazza, J. P., Zhi, W., Nemeth, P., Srere, P. A., and Evans, C. T. (1990) Mutation of essential catalytic residues in pig citrate synthase. *Biochemistry 29*, 7557–7563.
25. Karpusas, M., Holland, D., and Remington, S. J. (1991) 1.9 Å structures of ternary complexes of citrate synthase with D- and L-malate: mechanistic implications. *Biochemistry 30*, 6024–6031.
26. Karpusas, M., Branchaud, B., and Remington, S. J. (1990) Proposed mechanism for the condensation reaction of citrate synthase: 1.9-Å structure of the ternary complex with oxaloacetate and carboxymethyl coenzyme A. *Biochemistry 29*, 2213–2219.
27. Gu, Z., Drueckhammer, D. G., Kurz, L., Liu, K., Martin, D. P., and McDermott, A. (1999) Solid state NMR studies of hydrogen bonding in a citrate synthase inhibitor complex. *Biochemistry 38*, 8022–8031.
28. Usher, K. C., Remington, S. J., Martin, D. P., and Drueckhammer, D. G. (1994) A very short hydrogen bond provides only moderate stabilization of an enzyme-inhibitor complex of citrate synthase. *Biochemistry 33*, 7753–7759.
29. Kurz, L. C., Drysdale, G. R., Riley, M. C., Evans, C. T., and Srere, P. A. (1992) Catalytic strategy of citrate synthase: effects of amino acid changes in the acetyl-CoA binding site on transition-state analog inhibitor complexes. *Biochemistry 31*, 7908–7914.
30. Johansson, C. J., and Pettersson, G. (1977) Substrate-inhibition by acetyl-CoA in the condensation reaction between oxaloacetate and acetyl-CoA catalyzed by citrate synthase from pig heart. *Biochim. Biophys. Acta 484*, 208–215.
31. Johnson, K. A. (1992) Transient-state kinetic analysis of enzyme reaction pathways, in The Enzymes , Vol. 20, pp 1−61, Academic Press, New York.
32. Kurz, L. C., Ackerman, J. J. A., and Drysdale, G. R. (1985) Evidence from ^{13}C NMR for polarization of the carbonyl of oxaloacetate in the active site of citrate synthase. *Biochemistry 24*, 452–457.
33. Kurz, L. C., and Drysdale, G. R. (1987) Evidence from Fourier transform infrared spectroscopy for polarization of the carbonyl of oxaloacetate in the active site of citrate synthase. *Biochemistry 26*, 2623–2627.
34. van der Kamp, M. W., Perruccio, F., and Mulholland, A. J. (2007) Substrate polarization in enzyme catalysis: QM/MM analysis of the effect of oxaloacetate polarization on acetyl-CoA enolization in citrate synthase. *Proteins 69*, 521–535.
35. Wiegand, G., Remington, S., Deisenhofer, J., and Huber, R. (1984) Crystal structure analysis and molecular model of a complex of citrate synthase with oxaloacetate and *S*-acetonyl-coenzyme A. *J. Mol. Biol. 174*, 205–219.
36. Remington, S., Wiegand, G., and Huber, R. (1982) Crystallographic refinement and atomic models of two different forms of citrate synthase at 2.7 and 1.7 Å resolution. *J. Mol. Biol. 158*, 111–152.
37. Cornforth, J. W., Redmond, J. W., Eggerer, H., Buckel, W., and Gutschow, C. (1969) Asymmetric methyl groups, and the mechanism of malate synthase. *Nature 221*, 1212–1213.
38. Kresge, A. J. (1977) Magnitude of primary hydrogen isotope effects, in Isotope effects on enzyme-catalyzed reactions (Cleland, W. W., O'Leary, M. H., and Northrop, D. B., Eds.) pp 37−63, University Park Press, Baltimore, MD.
39. Kiefer, P. M., and Hynes, J. T. (2006) Interpretation of primary kinetic isotope effects for adiabatic and nonadiabatic proton-transfer reactions in a polar environment, in Isotope effects in chemistry and biology (Kohen, A., and Limbach, H.-H., Eds.) pp 549−578, CRC Press, Boca Raton, FL.
40. Clark, J. D., O'Keefe, S. J., and Knowles, J. R. (1988) Malate synthase: proof of a stepwise Claisen condensation using the double-isotope fractionation test. *Biochemistry 27*, 5961–5971.
41. Northrop, D. B., and Cho, Y. K. (2000) Effects of high pressure on solvent isotope effects of yeast alcohol dehydrogenase. *Biophys. J. 79*, 1621–1628.
42. Schowen, K. B. J. (1978) Solvent hydrogen isotope effects, in Transition states of biochemical processes (Gandour, R. D., and Schowen, R. L., Eds.) pp 225−283, Plenum Press, New York.
43. Mulholland, A. J., and Richards, W. G. (1997) Acetyl-CoA enolization in citrate synthase: a quantum mechanical/molecular mechanical (QM/MM) study. *Proteins 27*, 9–25.